ADVANCED FUNCTIONAL MATERIALS
www.afm-journal.de

# Mapping the Density of States Distribution of Organic Semiconductors by Employing Energy Resolved–Electrochemical Impedance Spectroscopy

*Heinz Bässler, Daniel Kroh, Franz Schauer, Vojtech Nádaždy, and Anna Köhler**

**Although the density of states (DOS) distribution of charge transporting states in an organic semiconductor is vital for device operation, its experimental assessment is not at all straightforward. In this work, the technique of energy resolved–electrochemical impedance spectroscopy (ER-EIS) is employed to determine the DOS distributions of valence (highest occupied molecular orbital (HOMO)) as well as electron (lowest unoccupied molecular orbital (LUMO)) states in several organic semiconductors in the form of neat and blended films. In all cases, the core of the inferred DOS distributions are Gaussians that sometimes carry low energy tails. A comparison of the HOMO and LUMO DOS of P3HT inferred from ER-EIS and photoemission (PE) or inverse PE (IPE) spectroscopy indicates that the PE/IPE spectra are by a factor of 2–3 broader than the ER-EIS spectra, implying that they overestimate the width of the distributions. A comparison of neat films of MeLPPP and SF-PDI$_2$ or PC(61)BM with corresponding blends reveals an increased width of the DOS in the blends. The results demonstrate that this technique does not only allow mapping the DOS distributions over five orders of magnitude and over a wide energy window of 7 eV, but can also delineate changes that occur upon blending.**

## 1. Introduction

Organic semiconductors (OSs) are the key active element in todays' photocopiers and are gaining increasing importance in opto-electronic devices such as organic lighting emitting diodes,[1–3] organic solar cells (OSCs)[4–6] and organic field effect transistors.[7] For practical reasons they are amorphous or polycrystalline films. This implies structural disorder. As a consequence, charge transport in OSs is slowed down as compared to that in counterpart perfect molecular crystals. It is well established that charge carriers move via incoherent hopping within a density of state (DOS) distribution.[8–11] The broader the DOS is, the lower is the charge carrier mobility and the higher is the associated activation energy as well as the time after which a dynamic process equilibrates, such as the motion of a sheet of charge carriers injected from an electrode. Mapping the DOS to determine the energies of the electron and hopping transporting states is therefore crucial for material characterization.[12,13]

Disorder in OSs is manifested in the broadening of their absorption and photoluminescence spectra of OS-films. It reflects (i) the local variation of the van der Waals coupling of a singlet or triplet state to the polarizable environment,[8] (ii) structural variations of a chromophore, for example, the variation length of the effective conjugation length of a conjugated polymer,[14] and (iii) dynamic effects such as thermally activated rotational or vibrational motion within the chromophore.[15,16] Such contributions toward energetic disorder will also affect the DOS of valence and conduction states that control hole and electron motion. Moreover, DOS distributions are likely to change when going from neat to blended films. A further source of broadening of the tail of an absorption of a

Prof. H. Bässler, Prof. A. Köhler
Bayreuth Institute of Macromolecular Research (BIMF)
University of Bayreuth
Bayreuth 95448, Germany
E-mail: anna.koehler@uni-bayreuth.de

D. Kroh, Prof. A. Köhler
Soft Matter Optoelectronics and Bavarian Polymer Insitute (BPS)
University of Bayreuth
Bayreuth 95448, Germany

Prof. F. Schauer
Faculty of Applied Informatics
Tomas Bata University in Zlín
Zlin 760 05, Czech Republic

Dr. V. Nádaždy
Institute of Physics
Slovak Academy of Sciences
Bratislava 845 11, Slovakia

Dr. V. Nádaždy
Centre for Advanced Material Application
Slovak Academy of Sciences
Bratislava 845 11, Slovakia

The ORCID identification number(s) for the author(s) of this article can be found under https://doi.org/10.1002/adfm.202007738.

© 2020 The Authors. Advanced Functional Materials published by Wiley-VCH GmbH. This is an open access article under the terms of the Creative Commons Attribution License, which permits use, distribution and reproduction in any medium, provided the original work is properly cited.

DOI: 10.1002/adfm.202007738

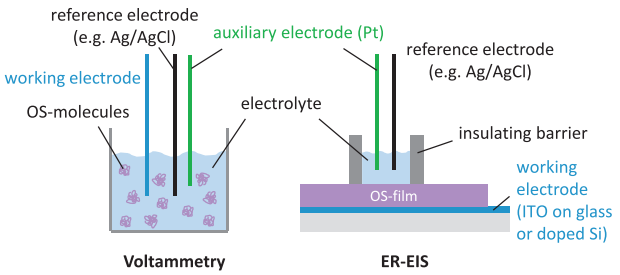


**Figure 1.** Schematic comparing the setups for a voltammetry measurement and an ER-EIS measurement.

semiconductor arises when absorption occurs not from the 0–0 vibrational state but—thermally activated—from phonon coupled states. This gives rise to exponential Urbach tails of the absorption spectra.[17,18] However, since the energies of Urbach tails are typically around a few meV only, this effect is relevant only in fairly ordered semiconductors such as molecular or inorganic crystals, or hybrid materials such as perovskites[19] and would otherwise be buried under static and dynamic level broadening.

Unfortunately, the DOS of valence and conduction states in OSs is not amenable to direct optical absorption as it is case in inorganic semiconductors. The reason is that—owing to the weak electronic coupling in OSs—photo-excitation creates excitons rather than charge carriers, so that the direct transition from the valence (HOMO) DOS to the conduction (LUMO) DOS is not observed. A simple way to estimate the degree of disorder in OSs is to measure the temperature dependence of hole and electron transport. However, this yields only upper values for the widths of relevant DOSs because both dynamic disorder and structural relaxation may contribute to broadening, beyond the already existing static distribution in the DOS.[10,11] Moreover, it does not provide information on the detailed structure of the DOS. An alternative method toward DOS mapping is photoemission (PE)[20] and inverse PE (IPE).[21,22] It is experimentally demanding and data analysis may be complicated because electrons emitted from different layers of the OS have slightly different energies since the polarization energies of molecules next to vacuum are diminished.[23,24]

In this work we apply the technique of energy resolved–electrochemical impedance spectroscopy (ER-EIS) to determine the DOS of selected OSs. ER-EIS is a novel electrochemical impedance technique bordering on voltammetry.[25,26] Usually, the organic semiconductor probed by voltammetry is dissolved in solution. In an ER-EIS measurement, in contrast, the OS is deposited as a film, where solid state effects prevail (**Figure 1**). Thus, the molecules are probed in the local environment of the film, so that the ER-EIS-spectrum is a direct reflection of the DOS of the hole (HOMO) and electron (LUMO) transporting states. In the current work we will use MeLPPP and P3HT as a donor-type conjugated polymer and PCBM and SF-PDI$_2$ as representative electron acceptors in the form of neat films as well as in blends. We will demonstrate that the ER-EIS technique does not only allow to map the DOS functions over as many as five decades but also to delineate changes which occur upon blending. We find that the examined DOS distributions are usually of Gaussian character but in case of PCBM there is an exponential tail.

## 2. The ER-EIS Experiment

ER-EIS is a spectroscopic method to map the electronic structure of an organic solid in the contact with an electrolyte via a redox-reaction.[27–30] It evolved out of the electrochemical impedance spectroscopy and advanced general voltammetric techniques such as square wave voltammetry[31–33] or other reported voltammetric modulation approaches.[31,34] We briefly outline its operational principle and refer to refs. [26,28] for further details. For the measurement, a 3-electrode electrochemical cell is used. Thus, a thin film, typically about 100 nm, of the OS is deposited by spin-coating onto a conducting substrate, in our case indium-tin-oxide (ITO) covered glass or doped Si. The OS film is covered by a liquid electrolyte that is contained by an inert, insulating frame. An Ag/AgCl reference and a Pt auxiliary wire electrode are inserted into the electrolyte, while the ITO or Si serves as working electrode. A DC voltage ramp between reference and working electrode is swept, modulated by an AC voltage of suitably chosen frequency, and the resulting current is recorded. The measured impedance $Z_{meas}$ is a result of the Helmholtz layer that forms at the electrolyte/OS interface when a voltage is applied. Reversible charge transfer from ions of the electrolyte to countercharges in the OS in the vicinity of the interface will occur once the applied voltage compensates the difference between the energies of the relevant states, and this gives rise to the real component of $Z_{meas}$. Under steady state conditions this interfacial recombination current has to be balanced by a current flowing through the OS that carries an exit contact, in our case the ITO or doped Si electrode. A crucial condition is that the rate limiting step must be charge exchange at the electrolyte/OS interface rather than the charge transport toward to the exit contact. This implies that the voltage drop across the OS bulk be negligible relative to the voltage required to drive the injection at the interface. In turn, this requires a percolating network of transport states and implies charge transport via drift and diffusion under space charge limited (SCL) conditions.

The setup for a ER-EIS measurement may appear similar to that of an electrochemical field-effect transistor.[35] In both cases, the organic semiconductor film is covered by an electrolyte with a Ag/AgCl reference electrode and a Pt auxiliary electrode inserted into it. However, there are several differences between the two methods. In the electrochemically gated field effect transistor, the recorded signal is typically the direct current flow from source to drain electrode while a potential is applied at the gate electrode. In these measurements, counterions that diffuse into the semiconductor from the electrolyte play a role. The electrochemical impedance measurement, in contrast, is conducted using an alternating current signal such as to prevent significant counterion effects. Further measures to avoid intercalation of ions include measuring the whole spectrum in two steps, always in a new electrochemical cell, with one measurement being used to obtain the branch for hole transporting states and one for the electron transporting states, as detailed in refs. [26–28].

Experimentally, the charge transfer resistance at the electrolyte/OS interface is measured by superimposing a periodic perturbation of the applied potential. Upon scanning the applied voltage one can assess the energetic position, and thus


© 2020 The Authors. Advanced Functional Materials published by Wiley-VCH GmbH

the distribution of the hole and electron transporting states depending on the applied voltage. The DOS function $g(E)$ in the semiconductor at the Fermi energy $E_F = eU$ can be extracted from the measured impedance

$$Z_{meas} = R_{ct} + \frac{1}{j\omega C_{sc}} \tag{1}$$

where

$$\left[R_{ct}(E_F)\right]^{-1} = e^2 S[A] V_f g(E_F) k_{et}(E_F) \tag{2}$$

is the differential charge transfer resistance and

$$C_{sc}(E_F) = \frac{\partial Q_{SC}}{\partial U_{SCLC}} = e^2 L S g(E_F) \tag{3}$$

is the differential space-charge capacity in the bulk of the polymer.[28] $L$ is the sample thickness, $S$ is the area of the working electrode, and $[A]$ is the concentration of the OS redox species dissolved in the solvent. $V_f$ is the volume fraction of respective charge carriers near the surface with an effective thickness of the acceptor/donor layer next to the interface of typically 1–2 nm.[36] The $k_{et}(E)$ is the electron-transfer rate.[37] The use of the charge-transfer resistance data $R_{ct}(E_F)$ (Equation (2)) and the space-charge capacitance data $C_{sc}(E_F)$ (Equation (3)) constitutes two complementary approaches, which probe different parts of the conjugated polymer film, both providing information on the DOS function $g(E_F)$. The $R_{ct}$ reflects the redox process that takes place near the surface of the OS and the electrolyte whereas $C_{SC}$ traces the bulk of the conjugated polymer film. For the data presented below, we evaluated the charge-transfer resistance data. We confirmed that the same results are obtained for the DOS function when evaluating the differential space-charge capacitance.

## 3. Results

### 3.1. The P3HT DOS Probed by Photoemission and by ER-EIS

In order to determine the electrical gap of a P3HT film Deibel et al.[22] had measured the spectra of PE as well IPE. They provide reference information on the DOS distribution. It was straightforward to apply the ER-EIS technique to study P3HT and compare the results, thereby extending our earlier work.[25,27,38] In **Figure 2**a we present the spectrum we obtain from our impedance measurements for the DOS function $g(E_F)$ while Deibel et al.'s results are shown in Figure 2b. For the sake of easy comparison the original PE and IPE spectra have been replotted on a semi-logarithmic scale. The edges to the spectra have been fitted to Gaussian lineshapes (see **Table 1**). It is gratifying that the tails of the Gaussians approximately coincide (see also the dashed lines in Figure 2). However, the PE and IPE spectra are significantly broader and the separation between their maxima has increased from 3.18 to 3.9 eV. We also note the smaller dynamic range of the PE/IPE measurement.

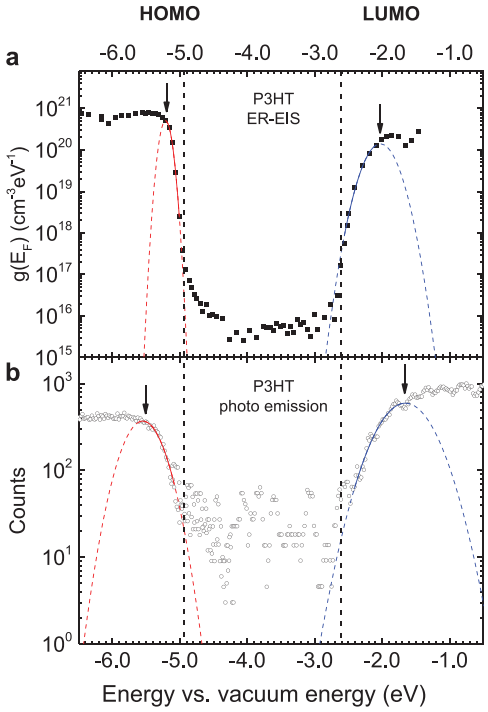


**Figure 2.** The DOS function $g(E_F)$ for HOMO and LUMO states of a P3HT film inferred from either a) ER-EIS or b) photoemission and inverse photoemission (data from Deibel et al.[22]). The colored dashed lines indicate Gaussian fits with the solid colored line indicating the data points considered in the fit. The arrows indicate the center position of the Gaussians. The black dashed lines serve to ease comparison between DOS tails obtained from both methods.

### 3.2. The Donor Polymer MeLPPP with a Fullerene and a Non-Fullerene Acceptor

In order to characterize the DOS distributions of a conjugated donor polymer and, importantly, to delineate changes that can occur upon blending we use the ladder-type MeLPPP. It is one of the least disordered polymers as evidenced by the narrow absorption and emission spectra.[16] This facilitates to uncover morphology-related changes of the DOS-distributions. As representative film-forming acceptors we use PC(61)BM and SF-PDI$_2$.

**Figure 3** shows the compilation of the ER-EIS spectra for the DOS function $g(E_F)$ for the hole and electron transporting states of radical cation and anion states. We attribute the high

**Table 1.** The center energy $E_0$ and the standard deviation $\sigma$ obtained from the Gaussian fits to the edges of the HOMO and LUMO attributed parts of the DOS function for a P3HT film. Also given is the energy gap $E_g = E_0$ (HOMO) – $E_0$ (LUMO).

| P3HT | | Photo-emission | ER-EIS |
|---|---|---|---|
| HOMO | $E_0$ [eV] | −5.55 | −5.21 |
| | $\sigma$ [meV] | 255 | 63 |
| LUMO | $E_0$ [eV] | −1.65 | −2.03 |
| | $\sigma$ [meV] | 355 | 168 |
| $E_g$ | [eV] | 3.90 | 3.18 |


© 2020 The Authors. Advanced Functional Materials published by Wiley-VCH GmbH

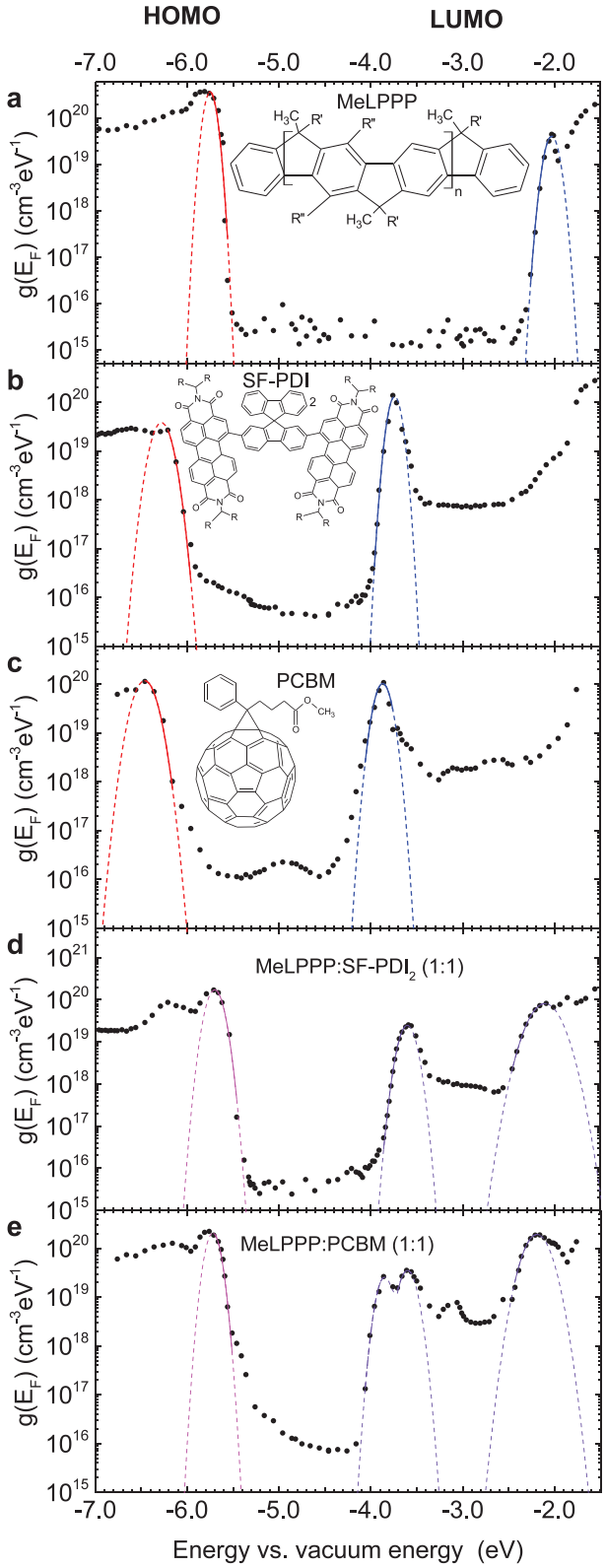


**Figure 3.** DOS function $g(E_F)$s for HOMO and LUMO states of neat films of a) MeLPPP, b) SF-PDI$_2$, c) PC(61)BM, d) MeLPPP:SF-PDI$_2$, and e) MeLPPP:PCBM blends, inferred from ER-EIS. The colored dashed lines indicate Gaussian fits with the solid colored line indicating the data points considered in the fit.

(low) energy edge of DOS function for the hole (electron) states to the HOMO (LUMO). The data derived from the spectra are summarized in **Table 2**. The spectra for a neat MeLPPP film are presented in Figure 3a. Both the parts of the DOS function attributed to the HOMO as well as the part attributed to the LUMO are of Gaussians extending over five decades in amplitude, recognizing, though, that it is principally difficult to distinguish whether a low energy tail has a Gaussian or an exponential shape. The standard deviations ($\sigma$) of HOMO- and LUMO-attributed $g(E_F)$ functions are 50 and 60 meV (see Table 2).

The HOMO-attributed part of the DOS function $g(E_F)$ of a SF-PDI$_2$ neat film is of Gaussian shape over two orders of magnitude but it carries a weak tail (Figure 3b) while the LUMO-attributed part of the DOS function $g(E_F)$ is also a perfect Gaussian with a standard deviation of 55 meV. The gap between the centers of the HOMO and LUMO attributed parts is 2.54 eV, that is, 0.17 eV higher than a literature value inferred from cyclic voltammetry.[39] Remarkably, the standard deviation of the optical absorption is about 150 meV, that is, significantly larger than the DOS values for the charge transporting states.

In Figure 3c we show the DOS function for a neat PC(61)BM film. Over two orders of magnitude the HOMO-attributed part is of Gaussian shape with $\sigma$ = 95 meV with an exponential tail while the LUMO-attributed part is a pure Gaussian with $\sigma$ = 65 meV. The electrical gap, defined by the separation between the maxima of the parts, is 2.6 eV.

In blends with MeLPPP and either PC(61)BM or SF-PDI$_2$ the high energy edge of the lower energy part of $g(E_F)$ is associated with the HOMO of the donor (MeLPPP) (Figure 3d,e)). The Gaussian character of the HOMO of MeLPPP is preserved but there is additional state broadening $\sigma$ (70 and 63 meV instead of 50 meV) and tail states appear at the high energy side of the HOMO roughly 0.3 eV above the center of the bulk-DOS. Their relative concentrations are roughly 0.001 (MeLPPP:SF-PDI$_2$) and 0.01 (MeLPPP:PCBM). In the blend, the lowest energy feature in the higher energy part of $g(E_F)$ is the LUMO of the acceptor, while the higher energy feature around −2 eV can be associated with the MeLPPP LUMO. In both cases there is a significant broadening of the LUMO of MeLPPP. Moreover, in the MeLPPP:PCBM blend, additional features can be discerned, centered at −3.60 and −3.10 eV, with $\sigma$ = 75 and 110 meV, respectively, that that are barely visible in neat PC(61)BM (see also **Figure 4**b below for ease of comparison, and Supporting Information).

## 4. Discussion

### 4.1. Comparison Between DOS Distribution Inferred from ER-EIS and Photoemission

The DOS distributions of HOMO and LUMO distributions of a neat P3HT film inferred from ER-EIS are of Gaussian shape with $\sigma$ parameters of 63 meV (HOMO) and 168 meV (LUMO). The electrical gap is 3.18 eV and—since the energy of the singlet exciton is about 2.1 eV, the exciton binding energy is about 1.1 eV, that is, close to that of MeLPPP and classic molecular crystals.[24] The fact that the width of the LUMO distribution is unusually


© 2020 The Authors. Advanced Functional Materials published by Wiley-VCH GmbH

**Table 2.** The center energy $E_0$ and the standard deviation $\sigma$ obtained from the Gaussian fits to the edges of the HOMO and LUMO attributed DOS functions $g(E_F)$ for neat films of MeLPPP, SF-PDI$_{,2}$ and PC(61)BM, as well as for the donor-acceptor blends. Also given is the energy gap $E_g = E_0$ (HOMO) − $E_0$ (LUMO). For the blends, center energies to multiple Gaussian fits are given for the LUMO, corresponding to donor or acceptor or different acceptor phases (c.f. Figure 3d,e).

| | | MeLPPP | SF-PDI$_2$ | PC$_{60}$BM | MeLPPP:SF-PDI$_2$ (1:1) | | MeLPPP:PC$_{60}$BM (1:1) | | |
|---|---|---|---|---|---|---|---|---|---|
| HOMO | $E_0$ [eV] | −5.75 | −6.28 | −6.46 | −5.70 | | −5.72 | | |
| | $\sigma$ [meV] | 50 | 83 | 95 | 70 | | 63 | | |
| LUMO | $E_0$ [eV] | −2.03 | −3.74 | −3.87 | −3.60 | −2.10 | −3.85 | −3.60 | −1.99 |
| | $\sigma$ [meV] | 60 | 55 | 65 | 70 | 133 | 65 | 75 | 114 |
| $E_g$ | [eV] | 3.72 | 2.54 | 2.61 | 2.10 | 3.60 | 1.87 | 2.12 | 3.73 |

broad can be ascribed to the broader distribution of effective conjugation length in a P3HT film.[40] However, the PE and IPE spectra are significantly broader than the ER-EIS spectra, and the gap between the peak positions are increased from 3.18 to 3.9 eV. The observation that upon going from ER-EIS to PE/IPE the HOMO distribution increases from 60 to 260 meV and the LUMO distribution increases from 170 to 360 meV demonstrates that ER-EIS and PE/IPS monitor different phenomena. An ER-EIS experiment probes the electron-hole transfer directly from an electrolyte to the OS. On the other hand, PE probes the ejection of a highly excited electron into the gas-phase and IPE probes the dissipation of electrons upon entering the solid.[41] Therefore the respective response functions in PE and IPE are the convolutions of the DOS functions and the escape/dissipation functions. In the case of PE, electron ejection is likely to be affected by the electron scattering and the decrease of the polarization energy of an electron at the interface between the OS and vacuum.[23] Both effects will broaden the response function and increase the apparent ionization energy. A PE spectrum is, therefore, unable to probe the width of the DOS-distributions for HOMO states. Studies on charge transport and theoretical studies support this reasoning.[12] Suppose the width of the HOMO-DOS distribution of a P3HT film were as broad as 260 meV, then the hole mobility would—based upon the Gaussian disorder model (ref. 8)—be about $10^{-17}$ cm$^2$ Vs$^{-1}$, in striking disagreement with experiment.[42,43] There is indeed consensus that width of distributions of hole and electron transporting states are typically around 100 meV.[44]

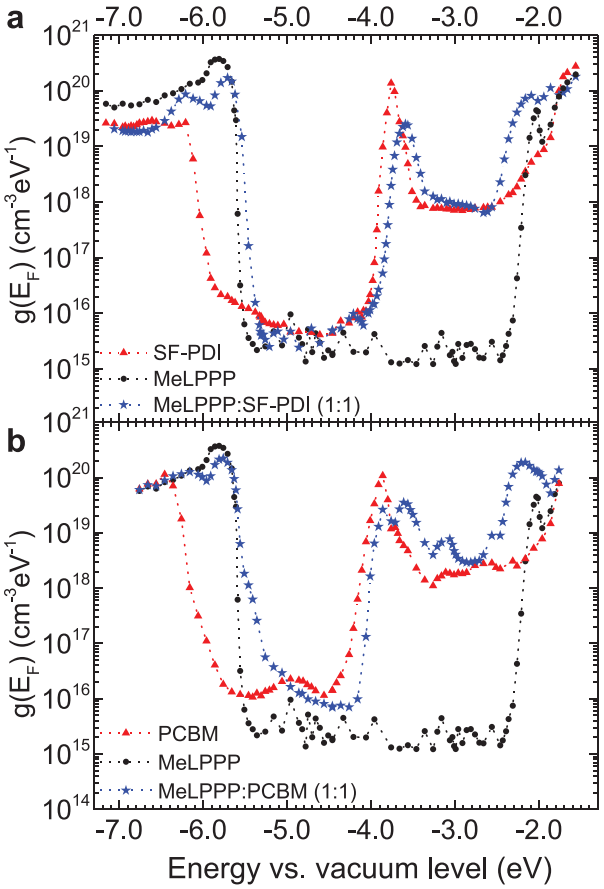


**Figure 4.** Comparison of the DOS distributions of neat and blends obtained by ER-EIS for the neat films and for blends of MeLPPP with a) SF-PDI$_2$ or b)PC(61)BM. Dotted lines between the data points (symbols) mere serve to guide the eye.

### 4.2. Neat Films

In all cases the DOS functions of HOMO and LUMO states shown in Figure 3a–c are either full Gaussians or Gaussians that extend into weak tails with a characteristic energy of about 100 meV, that is, at least one order of magnitude larger than those of typical Urbach tails. Provided that the DOS function indeed reflects the DOS, this confirms that the DOS widths are due to static and dynamic disorder. The simplest approach to analyze the DOS distributions is the point-site concept.[8] It implies that either a point charge or a localized exciton polarize their environment via van der Waals coupling with coupling energies featuring an $r^{-4}$ (charge) and $r^{-6}$ (exciton) dependence on distance, respectively. Imposing a random distribution of the intermolecular separations translates into a distribution of Gaussian character because the polarization energies depend on a large number of coordinates each varying randomly and therefore the central limit theorem applies. It is easy to show that in this case the ratio of the standard deviations of the DOSs for charges ($\sigma_c$) and excitons ($\sigma_{exc}$) is $\sigma_c/\sigma_{exc} = 4P_c/6P_{exc}$ where $P_c$ and $P_{exc}$ are the polarization energies of charges and excitons, respectively.

A vapor deposited PC(61)BM film is a system in which the point-site model may provide a reasonable estimate for analyzing the DOS distributions of charge carriers and excitons. The electron affinity (EA) of PC(61)BM in the gas-phase and in the solid are 2.63–2.65 eV[45,46] and 3.84 eV,[47] respectively.


© 2020 The Authors. Advanced Functional Materials published by Wiley-VCH GmbH

The difference between the EA values in the gas-phase and the solid, that is, the polarization energy of a radical anion, is 1.2 eV like in many organic solids.[24] The value for the EA in solid PC(61)BM, −3.86 agrees well with the average value measured by different techniques. The standard deviations ($\sigma$) of the HOMO/LUMO-DOSs inferred from ER-EIS spectra are 95 and 90 meV, respectively. They are significantly lower than the value 130 meV that Tummals et al.[13] obtained from molecular dynamics simulations. On the other hand, the $\sigma$ value for the singlet excitons in PC(61)BM, inferred from the delayed fluorescence spectra at 295 K, is only 40 meV.[48] To be consistent with the point site model (see above) polarization energy of the singlet exciton in the solids had to be 350 meV. This is indeed the difference between the energy of the singlet state of the anthracene molecule in the gas-phase (3.45 eV)[49] and in the solid (3.1 eV),[24] which can be taken as a reference value (in lack of corresponding data on PC(61)BM).

The width of the LUMO-DOS should be reflected in the temperature dependence of the electron mobility. From temperature dependent SCL electron transport in PC(61)BM diodes Mihailetchi et al.[50] concluded that electron transport is consistent with the extended Gaussian disorder model and extracted a $\sigma$ value of 77 meV. This value is 15% lower than the width of the LUMO-DOS. A possible reason for this discrepancy is that in the SCL transport mode tail states of the LUMO-DOS are partially filled. This should diminish the experimentally determined width of the electron DOS. Moreover, the film investigated by Mihailetchi et al. and our film have not been prepared using precisely the same deposition conditions, so that the film morphology can vary slightly.

The HOMO-DOS of a PC(61)BM film is of Gaussian shape over only two orders of magnitude and features a broader tail at higher energies. Such exponential tails have occasionally been observed.[51] They are a signature of traps that exist in systems in which the intrinsic HOMO-DOS is beyond 6 eV.[52] The position of the peak of the HOMO-DOS is 6.4 eV and is consistent with literature values.[53–56] Since the ionization energy in the gas phase is 7.59 eV,[57] the polarization energy of the radical cation in PBCM is close to 1.2 eV, that is, the same as the polarization energy of the radical anion. This yields an electrical gap of 2.6 eV while PE and IPE yield 2.37 eV.[56] From the action spectrum of intrinsic photo-generation we obtained $E_g = 2.45 \pm 0.05$ eV.[58] Combined with the fact that hole transport in PCBM is trap-limited we conjecture that the $E_g$ value inferred from the maxima of HOMO-LOMO DOSs of ER-EIS spectra refer to the intrinsic gap while the electrical gap determined from the tail of PE as well as photoconduction spectra are affected by the contribution of hole traps. Summing up, we argue that the point site model provides a reasonable basis for analyzing the DOSs for exciton as well as charge transporting states in a small molecule system such as vapor deposited PCBM film.

Let us now consider a SF-PDI$_2$ film. SF-PDI$_2$ is a more extended molecule as compared to PC(61)BM. The LUMO-DOS of SF-PDI$_2$ is a perfect Gaussian over 4 decades with a variance of 55 meV while the HOMO-DOS is somewhat broader ($\sigma = 83$ meV) and carries a weak tail. Remarkably the $\sigma$ value for the absorption spectrum, (shown in the SI) is 0.15 eV. This demonstrates that the DOS distributions for charge carriers can be narrower than those of neutral excitations. Even this also indicates that in this case the point-site model is unsuitable for estimating the DOS distribution for charge carriers based upon absorption or PL spectra because the exciton is more spread out than in a spherical molecule like PC(61)BM.[59]

Next we turn to the ER-EIS spectra for the HOMO and LUMO-DOS distributions of MeLPPP films. For MeLPPP the LUMO-DOS is a perfect Gaussian with a standard deviation of 60 meV while the HOMO-DOS is a somewhat distorted Gaussian with 50 meV. The absorption and fluorescence spectra are also Gaussians with a variance around 50 meV somewhat depending on film preparation.[60] It seems that the $\sigma$ values for charge carriers and singlet excitons are comparable. The point site model is clearly inappropriate for estimating the ratio of the spectral widths. This is because in conjugated polymers, the main contribution of disorder broadening stems from local variation of conjugations. This conjugation-induced variation translates into the site energies. A gratifying test of internal consistency is that the separation between the centers of the HOMO- and LUMO-DOSs is 3.8 eV and agrees with the threshold energy for intrinsic photo-generation.[61] Since the energy of the singlet exciton is 2.72 eV, the binding energy of exciton is about 1.2 eV like in conventional molecular solids.

In this context it is worth recalling earlier work on thermally stimulated luminescence (TSL) on thick films of MeLPPP. In such a TSL study one excites a sample at lower temperature to generate electron-hole pairs. They are meta-stable because electrons are deeply trapped. Upon raising the temperature from 5 K onward one observes delayed emission. It originates from the thermally activated release of holes from shallow intrinsic traps, that is, the HOMO-DOS, and subsequently recombines with trapped electrons. Therefore, the temperature dependence of the TSL signal reflects the HOMO-DOS of the MeLPPP host. By analyzing the TSL signal the shape and the width of the HOMO-DOS are recovered. The result confirms that at low temperatures (≈50 K) the DOS of a thick MeLPPP film has a Gaussian shape with $\sigma = 54$ meV.[62] This is in favorable agreement with the value of 50 meV inferred from the ER-EIS study.

We note that we do not observe any indication of trap states in the spectrum shown in Figure 3a. This is remarkable since electron-transport in MeLPPP has been found to be strongly trap-limited, with trap concentrations expected to be around $10^{18}$ cm$^{-3}$.[63] It is not fully clear why these traps are not evident in the ER-EIS spectra, and this is subjected to further investigation. Possibly this is related to the dominance of the counter-balancing hole current in MeLPPP, or poor injection of charges directly into the trap states.

### 4.3. Blended-Films

It is instructive to compare the DOS distributions of MeLPPP:PCBM and MeLPPP:SF-PDI$_2$ blends with those of the parent neat films (Figure 4). As expected, the upper HOMO-DOS it that of MeLPPP while the LUMO-DOS is that of either PCBM or SF-PDI$_2$. In the MeLPPP:PCBM blend there is marginal shift of the HOMO which acquires a tail. Of interest are three observations:

1) In the MeLPPP:PCBM blend the width of the LUMO-feature of MeLPPP is by a factor of about 2 broader than that in a


© 2020 The Authors. Advanced Functional Materials published by Wiley-VCH GmbH

neat film (114 vs 60 meV). Apparently, the incorporation of PBCM into domains of MeLPPP affects intra-grain ordering of polymer chains but, surprisingly, at a lesser degree in the HOMO distribution than in the LUMO distribution.

2) In the case of MeLPPP:SF-PDI$_2$ the HOMO/LUMO-DOS distributions bear out a global upward shift of about 0.1 eV and a ≈20% increase in width without any indication of specific aggregation occurring.
3) The weak, barely noticeable shoulder at −3.60 eV in the LUMO of PCBM becomes stronger in the blend with MeLPPP, so that it appears as a peak with the same intensity than the −3.85 eV peak of the LUMO in the neat PCBM. We tentatively assign the −3.85 eV feature to crystal-like domains and the −3.60 eV feature to more disordered PCBM. The rationale behind this reasoning is that upon progressive ordering the ionization energy of a solid decreases. Formation of ordered domains of PCBM in bulk-hetero junction OSCs in addition to more amorphous and possibly even intercalated structures is a well-established phenomenon.[64–66] In passing we note that the feature at −3.10 eV has also acquired more intensity compared to the neat PCBM film. Since this is more than half of an eV above the features attributed to LUMOs of differently ordered PCBM morphologies, we consider the −3.10 eV feature is more likely to arise from some different orbital.

## 5. Conclusions

Since that for PCBM both the ionization energy and the EA have been measured in the gas-phase employing PE techniques, the ER-EIS spectrum of a PCBM film provides values for the polarization energies of radical cations and anions as well as their standard deviations of the pertinent DOS distributions. Combined with PL spectroscopy we conclude that the simple point-site model, which rests upon the notion that disorder originates from of fluctuations of van der Waals coupling, is enough to understand disorder effects in PCBM. This is in contrast with films of conjugated polymers because there is an additional spreading of site energies due statistical variations of the effective conjugations length. The mutual consistence between different probes of disorder phenomena demonstrates that impedance spectroscopy is indeed a valuable technique to map the DOS distributions for charge carriers. Its particular advantage is that it allows mapping the DOS over five orders of magnitude. Its dynamic range is thus greater than that of PE spectroscopy and it is much cheaper and easier to employ.

We find that in all systems we looked at, the central portion of measured HOMO and LUMO distributions are of Gaussian shape, occasionally carrying broader tails that are associated with extrinsic defects and can act as charge carrier traps. Importantly, the ER-EIS technique is able to interrogate the DOS distributions in neat films as well as in blends. It is therefore a method to probe changes in the HOMO/LUMO distributions upon blending, albeit subject to the condition that there is a percolation path of charges across the film. An example is the broadening of the LUMO-DOS of MeLPPP upon blending with PCBM.

By comparing DOS distributions of a P3HT film inferred from PE and electrochemical impedance measurements, respectively, we find that widths of the DOS distributions determined using PE and IPE are typically by a factor 2–3 larger than those inferred from ER-EIS spectra The likely reason is that in the former case there is additional spectral broadening in the course of electron ejection from the OS to vacuum (PE) and dissipation of the excess energy in the injected electron (IPE). Therefore, PE and IPE overestimate the disorder in an OS.

## 6. Experimental Section

For the ER-EIS method, the electrochemical microcells had a volume of about ≈200 µl. The active organic semiconductor was deposited on top of either an ITO covered glass or highly doped Si (n+ or p+) substrates with deposited organic semiconductor thin film. The solution of 0.1 M TBAPF6 in anhydrous acetonitrile was used as the supporting electrolyte. The active organic semiconductor electrode area was 12 mm$^2$. The potential of the working electrode with respect to the reference Ag/AgCl electrode was controlled via a potentiostat. A Pt wire was used as the counter electrode. The potential recorded with respect to the reference Ag/AgCl electrode was recalculated to the local vacuum level assuming the Ag/AgCl energy versus vacuum value of 4.66 eV. An impedance/gain-phase analyzer, Solartron analytical, model 1260 (Ametek, Berwyn, USA), run in the usual three-electrode regime. The AC harmonic voltage signal frequency was usually 0.5 Hz, its rms value was 100 mV, and the sweep rate of the DC voltage ramp was 10 mV s$^{-1}$. Bode and Cole–Cole diagrams in the frequency range of 0.01–1 MHz were used for the preliminary ER-EIS frequency adjustment.

## Supporting Information

Supporting Information is available from the Wiley Online Library or from the author.

## Acknowledgements

The authors are indebted to Prof. C. Deibel for sending the photoemission data and to Ulli Scherf for giving the MeLPPP. The research of V.N. was funded by VEGA Project No. 2/0081/18 and was performed during the implementation of the project Building-up Centre for advanced materials application of the Slovak Academy of Sciences, ITMS project code 313021T081 supported by the Research & Innovation Operational Programme funded by the ERDF.

## Conflict of Interest

The authors declare no conflict of interest.

## Keywords

organic electronics, organic solar cells, photoemission spectroscopy, voltammetry

Received: September 10, 2020
Revised: October 21, 2020
Published online:


© 2020 The Authors. Advanced Functional Materials published by Wiley-VCH GmbH

[1] M. A. Baldo, D. F. O'Brien, Y. You, A. Shoustikov, S. Sibley, M. E. Thompson, S. R. Forrest, *Nature* **1998**, *395*, 151.
[2] J. Kido, M. Kimura, K. Nagai, *Science* **1995**, *267*, 1332.
[3] A. Köhler, H. Bässler, *Electronic Processes in Organic Semiconductors: An Introduction*, John Wiley & Sons, Hoboken, NJ **2015**.
[4] O. Inganäs, *Adv. Mater.* **2018**, *30*, 1800388.
[5] S. H. Park, A. Roy, S. Beaupre, S. Cho, N. Coates, J. S. Moon, D. Moses, M. Leclerc, K. Lee, A. J. Heeger, *Nat. Photonics* **2009**, *3*, 297.
[6] K. Vandewal, S. Albrecht, E. T. Hoke, K. R. Graham, J. Widmer, J. D. Douglas, M. Schubert, W. R. Mateker, J. T. Bloking, G. F. Burkhard, A. Sellinger, J. M. J. Frechet, A. Amassian, M. K. Riede, M. D. McGehee, D. Neher, A. Salleo, *Nat. Mater.* **2014**, *13*, 63.
[7] J. Zaumseil, H. Sirringhaus, *Chem. Rev.* **2007**, *107*, 1296.
[8] H. Bässler, *Phys. Status Solidi B* **1993**, *175*, 15.
[9] W. F. Pasveer, J. Cottaar, C. Tanase, R. Coehoorn, P. A. Bobbert, P. W. M. Blom, D. M. de Leeuw, M. A. J. Michels, *Phys. Rev. Lett.* **2005**, *94*, 206601.
[10] I. I. Fishchuk, A. Kadashchuk, S. T. Hoffmann, S. Athanasopoulos, J. Genoe, H. Bässler, A. Köhler, *Phys. Rev. B* **2013**, *88*, 125202.
[11] X. de Vries, P. Friederich, W. Wenzel, R. Coehoorn, P. A. Bobbert, *Phys. Rev. B* **2018**, *97*, 075203.
[12] G. Tirimbo, X. de Vries, C. H. L. Weijtens, P. A. Bobbert, R. Coehoorn, B. Baumeier, T. Neumann, *Phys. Rev. B* **2020**, *101*, 035402.
[13] N. R. Tummala, Z. L. Zheng, S. G. Aziz, V. Coropceanu, J. L. Bredas, *J. Phys. Chem. Lett.* **2015**, *6*, 3657.
[14] O. Narwark, S. C. J. Meskers, R. Peetz, E. Thorn-Csanyi, H. Bässler, *Chem. Phys.* **2003**, *294*, 1.
[15] M. B. Johnston, L. M. Herz, A. L. T. Khan, A. Köhler, A. G. Davies, E. H. Linfield, *Chem. Phys. Lett.* **2003**, *377*, 256.
[16] M. Marcus, J. D. Milward, A. Köhler, W. Barford, *J. Phys. Chem. A* **2018**, *122*, 3621.
[17] F. Urbach, *Phys. Rev.* **1953**, *92*, 1324.
[18] S. De Wolf, J. Holovsky, S. J. Moon, P. Loper, B. Niesen, M. Ledinsky, F. J. Haug, J. H. Yum, C. Ballif, *J. Phys. Chem. Lett.* **2014**, *5*, 1035.
[19] A. D. Wright, R. L. Milot, G. E. Eperon, H. J. Snaith, M. B. Johnston, L. M. Herz, *Adv. Funct. Mater.* **2017**, *27*, 1700860.
[20] W. R. Salaneck, C. B. Duke, W. Eberhardt, E. W. Plummer, H. J. Freund, *Phys. Rev. Lett.* **1980**, *45*, 280.
[21] S. Krause, M. B. Casu, A. Scholl, E. Umbach, *New J. Phys.* **2008**, *10*, 085001.
[22] C. Deibel, D. Mack, J. Gorenflot, A. Scholl, S. Krause, F. Reinert, D. Rauh, V. Dyakonov, *Phys. Rev. B* **2010**, *81*, 085202.
[23] C. B. Duke, T. J. Fabish, A. Paton, *Chem. Phys. Lett.* **1977**, *49*, 133.
[24] M. Pope, C. E. Swenberg, *Electronic Processes in Organic Crystals and Polymers*, 2nd ed., Oxford University Press, Oxford **1999**.
[25] F. Schauer, *J. Appl. Phys.* **2020**, *128*, 150902.
[26] F. Schauer, V. Nadazdy, K. Gmucova, *J. Appl. Phys.* **2018**, *123*, 161590.
[27] V. Nadazdy, F. Schauer, K. Gmucova, *Appl. Phys. Lett.* **2014**, *105*, 142109.
[28] F. Schauer, V. Nadazdy, K. Gmucova, T. Vary, *J. Appl. Phys.* **2018**, *124*, 165702.
[29] S. Athanasopoulos, F. Schauer, V. Nadazdy, M. Weiss, F. J. Kahle, U. Scherf, H. Bässler, A. Köhler, *Adv. Energy Mater.* **2019**, *9*, 1900814.
[30] D. Beljonne, J. Cornil, *Multiscale Modelling of Organic and Hybrid Photovoltaics*, Springer, Berlin **2014**.
[31] C. E. D. Chidsey, R. W. Murray, *J. Phys. Chem.* **1986**, *90*, 1479.
[32] D. D. Macdonald, *Electrochim. Acta* **2006**, *51*, 1376.
[33] A. J. Bard, L. R. Faulkner, *Electrochemical Methods: Fundamentals and Applications*, 2nd ed., John Wiley & Sons, Hoboken, NJ **2001**.
[34] R. E. M. Willems, C. H. L. Weijtens, X. de Vries, R. Coehoorn, R. A. J. Janssen, *Adv. Energy Mater.* **2019**, *9*, 1803677.
[35] I. N. Hulea, H. B. Brom, A. J. Houtepen, D. Vanmaekelbergh, J. J. Kelly, E. A. Meulenkamp, *Phys. Rev. Lett.* **2004**, *93*, 166601.
[36] J. W. Ondersma, T. W. Hamann, *J. Am. Chem. Soc.* **2011**, *133*, 8264.
[37] R. A. Marcus, *Rev. Mod. Phys.* **1993**, *65*, 599.
[38] K. Gmucova, V. Nadazdy, F. Schauer, M. Kaiser, E. Majkova, *J. Phys. Chem. C* **2015**, *119*, 15926.
[39] J. Liu, S. S. Chen, D. P. Qian, B. Gautam, G. F. Yang, J. B. Zhao, J. Bergqvist, F. L. Zhang, W. Ma, H. Ade, O. Inganas, K. Gundogdu, F. Gao, H. Yan, *Nat. Energy* **2016**, *1*, 16089.
[40] F. Panzer, H. Bässler, A. Köhler, *J. Phys. Chem. Lett.* **2017**, *8*, 114.
[41] N. V. Smith, *Rep. Prog. Phys.* **1988**, *51*, 1227.
[42] H. Sirringhaus, P. J. Brown, R. H. Friend, M. M. Nielsen, K. Bechgaard, B. M. W. Langeveld-Voss, A. J. H. Spiering, R. A. J. Janssen, E. W. Meijer, P. Herwig, D. M. de Leeuw, *Nature* **1999**, *401*, 685.
[43] P. Pingel, A. Zen, R. D. Abellon, F. C. Grozema, L. D. A. Siebbeles, D. Neher, *Adv. Funct. Mater.* **2010**, *20*, 2286.
[44] V. Coropceanu, J. Cornil, D. A. da Silva, Y. Olivier, R. Silbey, J. L. Bredas, *Chem. Rev.* **2007**, *107*, 926.
[45] B. W. Larson, J. B. Whitaker, X. B. Wang, A. A. Popov, G. Rumbles, N. Kopidakis, S. H. Strauss, O. V. Boltalina, *J. Phys. Chem. C* **2013**, *117*, 14958.
[46] J. Mort, M. Machonkin, I. Chen, R. Ziolo, *Philos. Mag. Lett.* **1993**, *67*, 77.
[47] H. Yoshida, *J. Phys. Chem. C* **2014**, *118*, 24377.
[48] F. J. Kahle, A. Rudnick, H. Bässler, A. Köhler, *Mater. Horiz.* **2018**, *5*, 837.
[49] E. M. Lottner, A. Slenczka, *J. Phys. Chem. A* **2020**, *124*, 311.
[50] V. D. Mihailetchi, J. K. J. van Duren, P. W. M. Blom, J. C. Hummelen, R. A. J. Janssen, J. M. Kroon, M. T. Rispens, W. J. H. Verhees, M. M. Wienk, *Adv. Funct. Mater.* **2003**, *13*, 43.
[51] S. L. M. van Mensfoort, J. Billen, S. I. E. Vulto, R. A. J. Janssen, R. Coehoorn, *Phys. Rev. B* **2009**, *80*, 033202.
[52] N. B. Kotadiya, A. Mondal, P. W. M. Blom, D. Andrienko, G. J. A. H. Wetzelaer, *Nat. Mater.* **2019**, *18*, 1182.
[53] J. H. Seo, S. J. Kang, C. Y. Kim, S. W. Cho, K. H. Yoo, C. N. Whang, *Appl. Surf. Sci.* **2006**, *252*, 8015.
[54] J. Niederhausen, P. Amsalem, A. Wilke, R. Schlesinger, S. Winkler, A. Vollmer, J. P. Rabe, N. Koch, *Phys. Rev. B* **2012**, *86*, 081411.
[55] K. Akaike, K. Kanai, H. Yoshida, J. Tsutsumi, T. Nishi, N. Sato, Y. Ouchi, K. Seki, *J. Appl. Phys.* **2008**, *104*, 023710.
[56] Z. L. Guan, J. B. Kim, H. Wang, C. Jaye, D. A. Fischer, Y. L. Loo, A. Kahn, *Org. Electron.* **2010**, *11*, 1779.
[57] H. Steger, J. Holzapfel, A. Hielscher, W. Kamke, I. V. Hertel, *Chem. Phys. Lett.* **1995**, *234*, 455.
[58] T. Hahn, S. Tscheuschner, C. Saller, P. Strohriegl, P. Boregowda, T. Mukhopadhyay, S. Patil, D. Neher, H. Bässler, A. Köhler, *J. Phys. Chem. C* **2016**, *120*, 25083.
[59] L. Yang, Y. S. Chen, S. S. Chen, T. Dong, W. Deng, L. Lv, S. N. Yang, H. Yan, H. Huang, *J. Power Sources* **2016**, *324*, 538.
[60] S. T. Hoffmann, H. Bässler, A. Köhler, *J. Phys. Chem. B* **2010**, *114*, 17037.
[61] S. Barth, H. Bässler, U. Scherf, K. Mullen, *Chem. Phys. Lett.* **1998**, *288*, 147.
[62] A. Kadashchuk, Y. Skryshevskii, A. Vakhnin, N. Ostapenko, V. I. Arkhipov, E. V. Emelianova, H. Bässler, *Phys. Rev. B* **2001**, *63*, 115205.
[63] E. Khodabakhshi, C. Ramanan, J. J. Michels, S. Bonus, D. Hertel, K. Meerholz, M. Forster, U. Scherf, P. W. M. Blom, *Adv. Electron. Mater.* **2020**, *6*, 2000082.
[64] N. C. Miller, E. Cho, R. Gysel, C. Risko, V. Coropceanu, C. E. Miller, S. Sweetnam, A. Sellinger, M. Heeney, I. McCulloch, J. L. Bredas, M. F. Toney, M. D. McGehee, *Adv. Energy Mater.* **2012**, *2*, 1208.
[65] N. C. Cates, R. Gysel, Z. Beiley, C. E. Miller, M. F. Toney, M. Heeney, I. McCulloch, M. D. McGehee, *Nano Lett.* **2009**, *9*, 4153.
[66] E. Czerwosz, P. Byszewski, R. Diduszko, H. Wronka, P. Dluzewski, E. Mizera, *J. Mater. Res.* **1996**, *11*, 3146.


© 2020 The Authors. Advanced Functional Materials published by Wiley-VCH GmbH